Polymer 282 (2023) 126160

Contents lists available at ScienceDirect

Polymer

journal homepage: www.elsevier.com/locate/polymer

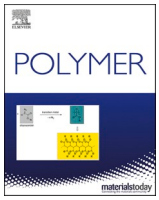

# Cationically photocured epoxy/polycaprolactone materials processed by solution electrospinning, melt electrowriting and 3D printing: Morphology and shape memory properties

I. Razquin [a], A. Iregui [a], M. Cobos [a], J. Latasa [b], A. Eceiza [c], K. González [c], L. Martin [d], A.J. Müller [a,e], A. González [a], L. Irusta [a,*]

[a] POLYMAT and Department of Polymers and Advanced Materials: Physics, Chemistry and Technology, University of the Basque Country UPV/EHU, PO Box 1072, 20080, Donostia-San Sebastián, Spain
[b] CIC NanoGUNE BRTA, Tolosa Hiribidea 76, 20018, Donostia-San Sebastián, Spain
[c] Group "Materials+Technologies", Department of Chemical and Environment Engineering, University of the Basque Country UPV-EHU, Plaza Europa 1, 20018, Donostia-San Sebastián, Spain
[d] Macrobehaviour-Mesostructure-Nanotechnology SGIker Service, University of the Basque Country UPV/EHU, Plaza Europa 1, 20018, Donostia-San Sebastián, Spain
[e] IKERBASQUE, Basque Foundation for Science, Plaza Euskadi 5, Bilbao, 48009, Spain

ARTICLE INFO

*Keywords:*
Epoxy/polycaprolactone blends
Solution electrospinning
Melt electrowriting (MEW)
FDM 3D printing
Shape memory
Shish-kebab morphology

ABSTRACT

Epoxy/polycaprolactone (PCL) blends containing cationic photo-initiator were prepared by both solution and melt blending. These materials were processed by solvent casting, solution electrospinning (SE), melt electrowriting (MEW), and Fused Deposition Modeling (FDM) 3D printing. The final materials were obtained after UV curing at room temperature. FTIR, and gel content measurements showed that all the materials were crosslinked and that the PCL was part of the network. The shape memory abilities (measured by DMA experiments) depended on the processing technique. Thus, the fixity and recovery ratios were optimal for electrospun fibers, while the 3D printed sample was not able to recover any shape, probably because of the poor adhesion between the printed layers. According to AFM images, samples obtained by MEW and 3D printing produced materials with spherulitic morphology, while solution electrospinning rendered fibers with Shish-Kebab-type crystalline morphology. The latter was highly anisotropic, and many chains were oriented along the nanofiber axis interdispersed with amorphous regions where the epoxy resin formed covalent links with the PCL chains. This morphology conferred extraordinary solvent resistance and shape memory properties to the electrospun mats. The latter manifested a very high affinity towards chloroform, and accordingly, they displayed potential applications as chloroform sensors.

## 1. Introduction

Polymer materials that are able to adopt a temporal shape and to recover the pristine permanent shape after the application of a stimulus such as temperature are called shape memory materials [1–3]. These materials present a large number of applications in different fields, such as biomedicine [4] and automobile engineering [5]. One of the strategies to obtain this type of polymer consists on preparing a bicomponent material in which one of the constituents forms a cross-linked network, responsible for the permanent shape of the material, while the other presents a thermal transition (either Tg or Tm) that allows the material to adopt different temporal shapes. An example of this type of structure that presents good shape memory properties is the epoxy resin/-polycaprolactone (PCL) blend [6,7].

The epoxy/PCL mixture is obtained by blending the epoxy prepolymer with the PCL in the presence of a curing agent and afterward crosslinking the resin (normally increasing the temperature) in the presence of the thermoplastic polymer. Depending on the crosslinking process, the final blend can present one-phase or two-phase morphology, which will determine the final properties of the material [8]. In most of the literature studying this blend, the epoxy, and PCL are blended by solvent casting [9]. However, to find a real application, melt blending is more appropriate [10,11]. In addition, for this blend to be processed, it should be considered that the final material is obtained

* Corresponding author.
*E-mail address:* lourdes.irusta@ehu.es (L. Irusta).

https://doi.org/10.1016/j.polymer.2023.126160
Received 11 May 2023; Received in revised form 27 June 2023; Accepted 28 June 2023
Available online 8 July 2023

after a curing reaction that will determine the final shape. This fact makes difficult the use of different processing techniques, such as electrospinning [12] and additive manufacturing [13], since the shape of the material can change as a consequence of the curing reaction.

PCL is a semi-crystalline polymer with a melting temperature close to 60 °C. The neat material exhibits a very fast crystallization rate from solution or from the melt state. The ability of PCL to crystallize in its blends with the epoxy resin depends on the miscibility between both components [10] which is related to the curing agent and curing mechanism of the epoxy resin as well as to the curing temperature. Accordingly, when the blend is cured at high temperatures and using amine-type crosslinking agents, miscible or non-miscible blends can be obtained depending on the employed diamine [10,14]. Previous research in our group [6] has shown that the epoxy/PCL blend cured with 4,4′-Diaminodiphenylmethane (DDM) is miscible and presents shape memory properties despite the fact that the PCL is not able to crystallize. However, if the target is to obtain good shape memory properties, the systems where the PCL is able to crystallize are more appropriate.

Cationic photopolymerization of epoxy resin has also been employed to obtain shape memory epoxy/PCL blends [15,16]. This polymerization process could proceed at room temperature and accordingly when the PCL is in the solid crystalline state. Previous results of our group have shown that when crosslinking proceeds at room temperature, the curing is obtained in the amorphous regions of the PCL in which the epoxy resin is found and that the crosslinked network obtained confines the semi-crystalline regions of the PCL, giving rise to a spherulitic pattern in films obtained by casting [17].

In previous work, using room temperature photocured epoxy/PCL blend, shape memory films and fibers were obtained by solvent casting and solution electrospinning [12,18]. The effect of different blend parameters (such as the blend composition) and electrospun parameters (voltage, flow rate) was studied to optimize the shape memory effect of the fibers. However, it is worth mentioning that preliminary non-published data of our group showed that electrospun fibers present superior solvent resistance and shape memory properties compared to films obtained by casting.

Considering this background, the objective of the present work was to understand why the photopolymerized PCL/epoxy blends obtained by solution electrospinning show better properties than their casting-processed counterparts. In addition, the behavior of materials processed without the participation of solvents via two additive manufacturing techniques, melt electrowriting (MEW) and Fused Deposition Modeling (FDM) 3D printing was analysed. The results of the present paper showed for the first time that the strong electric field applied during the solution electrospinning process originated the formation of Shish-Kebab-type crystalline morphology. This morphology conferred extraordinary solvent resistance and shape memory properties to the electrospun mats in comparison to the materials obtained by additive manufacturing.

## 2. Materials and methods

### 2.1. Materials

Bisphenol A diglycidyl ether (DGEBA, Mw = 340.41 g $mol^{-1}$), 2,2-dimethoxy-2-phenyl-acetophenone (DMPA), bis(4-*tert*-butylphenyl) iodonium hexafluorophosphate (IHPF), chloroform (99%), dimethylformamide (DMF) (99%) and acetone (99%) were supplied by Sigma Aldrich. Linear poly (ε-caprolactone) (PCL, Mn = 50.000 g $mol^{-1}$) was purchased from Perstorp, Malmö, Sweden. All materials were used as received.

### 2.2. Preparation of the mixtures

For the solution electrospinning process, a 20 wt% solution was prepared following the next procedure. 2.97 g of PCL and 2.97 g of DGEBA were dissolved in 25 mL of an acetone/DMF 3/1 vol mixture (16.67 g acetone and 8.33 g of DMF). Then, the solution was heated to 50 °C and stirred for 4 h. When the solution was homogeneous, 22 mg of DMPA (sensitizer) and 47 mg of IHFP (photoinitiator) were added, and the solution was kept in the dark.

Films were obtained by casting from a 5 wt% chloroform solution. Thus, 0.97 g of DGEBA and 0.97 g of PCL were dissolved in 25 mL of chloroform. 7 mg of DMPA and 15 mg of IHPF were added to the solution. The solution was placed on a Teflon mould at room conditions, and after solvent removal, a film of around 300 μm thickness and 8 cm of diameter was obtained. The film was kept in the dark.

For MEW and 3D printing, the blends were prepared in bulk in a 200 mL three-neck glass reactor equipped with a mechanical stirrer and a condenser. An oil bath was used to control the temperature. All the blending processes took place in the dark. Thus, 40 g of DGEBA, 0.63 g of photoinitiator, and 0.3 g of sensitizer were poured into the reactor. The mixture was heated at 80 °C and mechanically stirred at 200 rpm for 1 h. When the mixture was homogeneous, the temperature was increased to 120 °C, and afterward, 40 g PCL were added, and the stirring was maintained for additional 2 h. The mixture was kept in the dark for 24 h before processing.

### 2.3. Manufacturing techniques

To carry out the electrospinning process, a set-up consisting of a 30 kV high voltage source (SPELLMAN CZE1000R), a syringe pump (Cole Parmer), and a metallic collector consisting of a 10 × 10 mm aluminium plate was used. Disposable 5 mL plastic syringes (N5 mL plastic syringes (NORM-JECT, Air Tite) and needles with a straight cut of 1.2 mm diameter (BD Microlance 18G × 1 ½) were used for all experiments. Applying a voltage of 9 kV, randomly oriented fibers were obtained. The distance between the collector and the needle tip was 15 cm, and the flow rate was 0.30 mL/h. With the aim of easily removing the fibers from the collector, sulphurated paper was placed on top of the collector. The sample was collected for 8 h, and afterward, it was detached from the collector and kept in the dark.

To obtain the 3D printed sample, first, the 50/50 wt DGEBA/PCL blend (containing the photoinitiator and photosensitizer) was introduced in a mini extruder (Haake MiniLab, Thermo Electron Corporation) at 55 °C and 10 rpm with 30 g $min^{-1}$ flow, obtaining a 1.53–1.54 mm diameter filament. The filament was kept in the dark for 24 h. Then it was introduced in the 3D Printer (Tumaker, Voladora NX) with a nozzle diameter of 0.6 mm and 65 °C temperature. The other printing parameters were set at: 30 °C bed temperature, 6 $mms^{-1}$ print speed, and distance between nozzle and bed of 0.4 mm. A rectangle with a length of 8 cm, width of 1 cm, and thickness of 1 mm was printed. After printing, the sample was kept in the dark.

Melt electrowriting (MEW) is a specific type of melt electrospinning. In MEW, the fibers are directed to the collector without a whipping effect in contrast to the solution electrospinning. This allows the fibers to be deposited, reproducing precise pre-designed patterns. For the MEW, the mixture was cut into pieces of around 0.5 mm diameter that were introduced in the Novaspider ProLab 3D designed by CICnanoGUNE to obtain a mesh with 300 μm between fibers and 500 μm of thickness. The material was processed at 125 °C, 2.7 kV, 3 mm distance between the head and the bed, and 200 mm/s print speed. The sample was kept in the dark.

### 2.4. Curing process

Samples were cured for 1 h on each side using a UV LED lamp (ThorLabs M365LP1) at 25 °C, with an intensity of 2 mW/$cm^2$ at 365 nm. Electrospum mats were removed from the collector and cured in the same way. This process was carried out in a dark box.

### 2.5. Characterization

The curing process was characterized by Fourier Transform Infrared Spectroscopy (Nicolet 6700 FTIR) with a single reflection Attenuated Total Reflectance ATR system (Specac Golden Gate, Orpington England) at 10 scans and 4 $cm^{-1}$ of resolution. The decrease of the band centred at 915 $cm^{-1}$, which was related to the bending vibration of the epoxy group, was used to calculate reaction conversion.

The thermal behaviour of the samples was analysed by Differential Scanning Calorimetry (DSC) (TA Instruments Q2000, New Castle DE USA). Three consecutive temperature scans were registered. In the heating scans (first and third), the samples were heated from −80 °C to 150 °C, at a heating rate of 10 °C$min^{-1}$, in standard mode. In the cooling scan (second), the sample was quenched to −80 °C at a rate of 50 °C$min^{-1}$.

The morphology of the samples was studied by Scanning Electron microscope (SEM) (Hitachi, TM3030Plus) at 15 KV. Before the analysis, samples were coated with gold (SC 500 Sputter Coater, Emscope).

Atomic Force Microscopy was employed to observe the crystalline morphology of the samples obtained by the different processing techniques. The morphology of electrospun samples was studied by placing the mats directly in an AFM Nanoscope IVa, (Digital Instruments). The MEW and 3D printed samples were cut with an ultramicrotome (Leica Ultracut R) before being analysed by AFM (Dimension Icon, Bruker). A standard tip TESP-V2, Bruker, f = 320 kHz, k = 37 N $m^{-1}$) was used for all the samples.

Gel content was determined by gravimetry, measuring the weight of the sample after extraction in chloroform at 100 °C for 1 h in a pressure vessel (200 Psi), using a microwave equipment (MARS5X, CEM Corporation).

Mesh integrity was determined by adding chloroform to the sample at 25 °C in a Petri dish. The behaviour of the sample when chloroform was added and after solvent removal was visually monitored.

Acetone and chloroform sorption of the mats obtained by solution electrospinning was registered in a gravimetric electro balance (Intelligent Gravimetric Analyzer IGA-2, Hiden Isochema), which can regulate the vapor pressure of the solvents at different temperatures. Approximately 40 mg of the electrospun mat were placed on the balance support, and, after vacuum was applied, the vapor partial pressure of the solvent was progressively increased, taking at least, 20 intermediate points between the vacuum and a solvent activity of 1 at 25 °C.

The shape memory properties were studied by a DMA Q800 (TA Instruments, New Castle, DE USA) in a force-controlled mode. The experiment consisted on three steps [19].

**Step 1.** The sample without force with an initial deformation (εi) was heated at 70 °C for 5 min. After this isothermal step, a force ramp from 0 to 2 N at a rate of 0.8 N $min^{-1}$ was applied and the programmed deformation (εp) was obtained.

**Step 2.** The static force was kept, and the sample was cooled from 70 °C to 0 °C at 3 °C $min^{-1}$ for 5 min. The elongation obtained after removing the force was defined as the fixed elongation (εf).

Step 3. Without tension, the sample was heated to 70 °C at a 5 °C $min^{-1}$ rate. When the final temperature was reached, the sample was maintained at this temperature for 30 min, and the final elongation was recorded by the DMA as the recovery deformation (εr).

The fixity and recovery ratios were calculated by employing Equations (1) and (2).

$$Fixity\ \% = \frac{\varepsilon_f - \varepsilon_i}{\varepsilon_p - \varepsilon_i} \times 100 \quad (1)$$

$$Recovery\ \% = \frac{\varepsilon_p - \varepsilon_r}{\varepsilon_p - \varepsilon_i} \times 100 \quad (2)$$

## 3. Results and discussion

### 3.1. Characterization of the samples

The curing process was studied using (FTIR-ATR) spectroscopy for the DGEBA/PCL blend processed by the different techniques before and after UV irradiation. The scale-expanded FTIR-ATR spectra of the sample obtained by MEW are shown in Fig. 1.

As observed in Fig. 1, the absorbance of the band at 915 $cm^{-1}$, corresponding to the epoxy group bending (marked with an arrow in the spectrum), was reduced after UV irradiation, which means that the epoxy ring was opened [20]. This result evidenced that as a consequence of the irradiation, the acid groups generated were able to start the epoxy cationic polymerization even if the sample was in the solid state. To calculate the conversion, the 915 $cm^{-1}$ band was normalized with the absorbance at 1500 $cm^{-1}$ (that did not change during the reaction).

Infrared spectra of all the processed samples were obtained, and the conversion was calculated using Equation (3).

$$X = \left(1 - \left(\frac{\left(\frac{A_{915}}{A_{1500}}\right)_t}{\left(\frac{A_{915}}{A_{1500}}\right)_{t_0}}\right)\right) \times 100 \quad (3)$$

where $A_{915}$ is the area of the band assigned to the epoxy group and $A_{1500}$ is the area of the aromatic ring stretching before ($t_0$) and after (t) irradiation. The obtained values for different samples are shown in Table 1.

As can be seen in Table 1, regardless of the processing techniques employed, high conversion values were obtained. Interestingly the smallest conversion was obtained for the sample manufactured by 3D printing. This result was related to the higher thickness of this sample. Moreover, the gel content for the different samples was similar and was around 80–90%. These values confirmed the high conversion of the epoxy crosslinking reaction. However, it is worth mentioning that regardless of the processing method, the gel content was clearly higher than the percentage of epoxy resin in the blend. Accordingly, part of the PCL remained insoluble after UV irradiation.

The curing mechanism of the epoxy resin in the presence of PCL has been studied previously [21] According to the literature, when only DGEBA is photocured, an activated chain end (ACE) mechanism occurs, while in mixtures with PCL, the activated monomer (AM) mechanism and transesterification reactions happen. Considering previous results of our research group [17] the transesterification reaction takes place in the amorphous region of the PCL because the crosslinking reaction

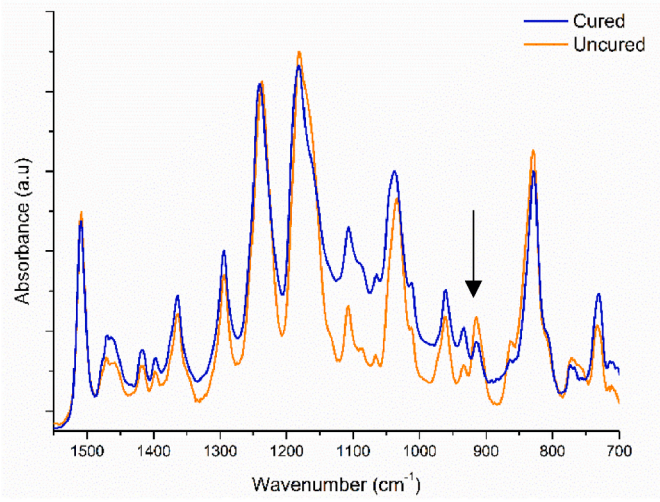


**Fig. 1.** Scale-expanded FTIR-ATR spectra of samples obtained by MEW before and after curing.

**Table 1**
Epoxy conversion of the different samples processed by different manufacturing techniques.

| Manufacturing technique | Conversion (%) | Gel content (%) |
|---|---|---|
| Solution electrospinning | 98 ± 1 | 84 ± 1 |
| MEW | 96 ± 1 | 83 ± 1 |
| Bulk film | 98 ± 1 | 87 ± 1 |
| 3D printing | 93 ± 1 | 85 ± 1 |

happens at room temperature (in order to maintain the morphology) [15,18,21]. Thus, the high gel content of the samples summarized in Table 1 is an evidence of the presence of the PCL in the insoluble fraction and therefore of the epoxy/PCL transesterification reaction. It is worth mentioning that the occurrence of the transesterification reaction did not produce significant changes in the infrared spectrum (carbonyl stretching region of the non-cured and cured samples are included in Fig. S1) since the final hydroxyl group reacted with the PCL ester giving rise to a new ester (with similar chemical structure) and a hydroxyl group.

### 3.2. Morphology

Fig. 2 shows the Scanning Electron Microscopy (SEM) images of the samples obtained by solution electrospinning, MEW and 3D printing.

The image of the electrospun mat (Fig. 2 (A)) showed a fiber-like morphology [18]. The size of the fibers was determined by the software ImageJ, and the calculated average diameter was 1.0 ± 0.4 μm.

The SEM image of the sample obtained by MEW is shown in Fig. 2 (B). As observed an ordered morphology was printed with fibers with 122 ± 31 μm diameter and 300 × 300 μm holes.

An Image of the 3D printed sample is shown in Fig. 2 (C). The sample showed a homogeneous surface without any mark of the printed layers of the 3D technique.

### 3.3. Thermal properties and crystallinity

The thermal behaviour of the samples was studied by DSC. The first heating scan for uncured and cured sample obtained by 3D printing is shown in Fig. 3.

As observed, before curing, the sample presented a glass transition temperature close to −21 °C. This transition was in between those of the neat components (PCL (Tg = −60 °C) and DGEBA (Tg = −33 °C)), which supported the hypothesis of miscibility between DGEBA and the amorphous regions of the PCL. Nevertheless, as observed in Fig. 3, the PCL still melted in the sample before curing, implying that the crystalline regions of PCL could not be dissolved by DGEBA. These PCL crystallites melted at a lower temperature than neat PCL because of the melting point depression caused by the interaction with the low molecular weight DGEBA which acted as a solvent. After curing, the glass transition temperature increased, but it overlapped with the melting endotherm of the PCL [22]. Moreover, the melting temperature increased after crosslinking [23]. This result evidenced that the photo-polymerization induced a phase separation between both

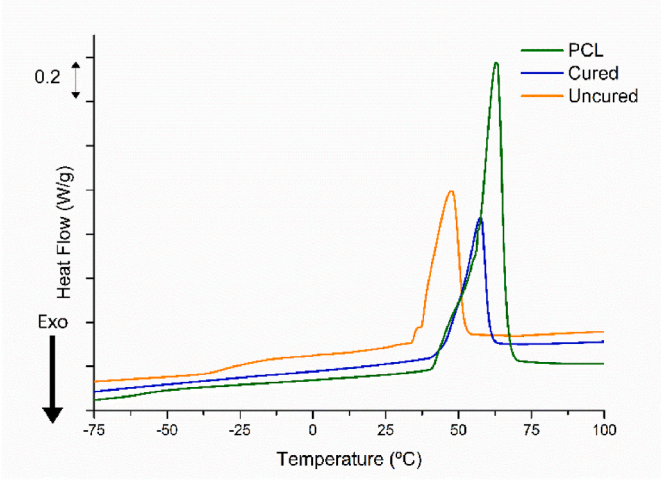


**Fig. 3.** DSC curves for the sample obtained by 3D technique before and after curing and pure PCL.

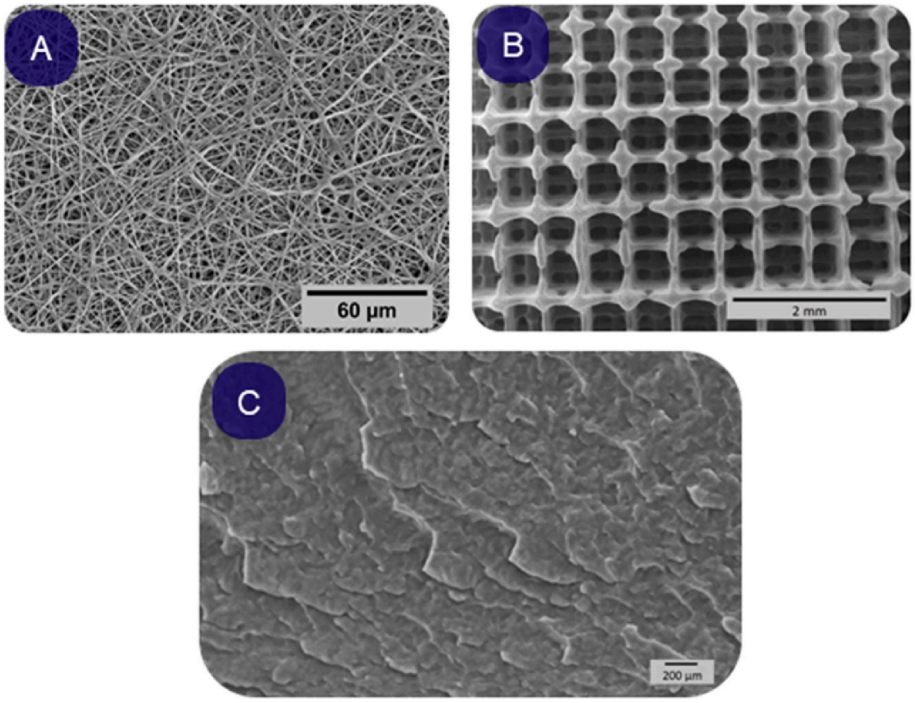


**Fig. 2.** SEM image of a solution electrospun mat (A), MEW (B), and a 3D printed specimen(C) after curing.

components, as observed in PCL/epoxy blend systems cured by Diamino diphenyl sulphone [24].

The same experiments were performed for all the samples, and the results are shown in Table 2.

As observed, before curing, the melting temperature and crystallinity degree of all the samples was lower than that of neat PCL because of the previously mentioned interaction with the low molecular weight DGEBA. In addition, both parameters did not show a clear dependence with the processing method. As expected, in the second scan, lower Tm and Xc values were obtained for all the samples because of the high cooling rate.

However, the curing process produced important changes in the melting temperature and crystallinity degree of the blends. Thus, regardless of the processing method, the melting temperature of all the cured samples was higher than that of their uncured counterparts. Likewise, the curing process increased the crystallinity degree of the samples. As explained in previous paragraphs, this result evidenced the phase separation produced during the epoxy photopolymerization process. Accordingly, the values of the Tm and Xc of the second scan of the cured samples were very close to those of neat PCL. It is worth mentioning that the 3D-printed sample showed lower Tm and Xc values than the samples processed by the other techniques, especially after the curing process. This result was related to the lower conversion of the crosslinking reaction (Table 1).

The crystalline morphology of the cured samples obtained by 3D printing, electrospinning, and MEW was studied by AFM. Fig. 4 shows the images of the samples processed by MEW and 3D printing.

As observed, the cured samples processed by 3D printing and MEW techniques presented a spherulitic crystalline morphology. Furthermore, the diameter of the spherulites did not depend on the processing technique since it was around 29 ± 3 μm and 30 ± 2 μm in 3D printing and MEW techniques, respectively. Therefore, the morphology of the samples remained similar even if the MEW samples were obtained under a high electrical field.

The AFM image of the sample obtained by solution electrospinning is shown in Fig. 5 and Fig. S2.

As observed the AFM images (Fig. 5, Fig. S2) we obtained are solid evidence of an oriented morphology that resembles in many cases the shish-kebab morphology that has been reported in the literature for analogous systems, where the material is produced under significant flow orientation [25,26]. The Shish-Kebab morphology is usually formed in polymers that crystallize from solution under complex flow fields that include very high shear and/or elongational components (and in some cases from the melt). In this case, we speculate that the orientation of the polymer chains was provoked by the electric field applied during the electrospinning process. Thus, the oriented polymer chains were able to crystallize along the fiber axes (Shish). These crystals were nucleating points for the crystallization of the Kebabs that happened perpendicularly to the spun fiber. In this way, the c-axis (or chain axis) of many polymer chains point in the direction of the electrospun fiber axis, as chains crystallize perpendicular to the lamellar surfaces (in the Kebabs) and mostly parallel to the fiber axis in the Shish central portion. The thickness of the Shish and Kebab structures was 18 ± 4 nm and 11 ± 2 nm, respectively. It is worth mentioning that the size of the Kebab is close to that reported in the literature for the lamellar thickness of neat PCL after isothermal crystallization [27].

This morphology was also observed by Lim et al. [28] in neat PCL fibers obtained by solution electrospinning. According to these authors, if the crystallization takes place during the flight of the fiber to the collector, better oriented lamellae are obtained favoring the production of the Shish-Kebab crystal morphology.

### 3.4. Solvent resistance of the materials

The solvent resistance of the cured materials processed by the different techniques was studied by swelling the samples in chloroform, as shown in Fig. 6.

As observed, after being immersed in chloroform, the sample obtained by solution electrospinning maintained its integrity. However, the samples obtained by the other processing techniques were broken after solvent treatment. The different crystalline morphology of the samples processed by the different techniques could be the origin of this behaviour.

In order for this behaviour to be explained, several considerations should be borne in mind. As DSC results have shown, the system was phase separated, and the epoxy resin was mixed with the amorphous regions of the PCL. Moreover, epoxy resin was cross-linked, and therefore it cannot be dissolved. In addition, the exchange reaction that took place between the resin and the PCL, integrated the PCL into the network structure [17]. This exchange reaction occurred in the amorphous regions of the blend as there was no epoxy resin in the crystalline regions. In addition, the cross-linked epoxy resin confined the crystalline regions of the PCL, as shown in previous papers [17], which could prevent the PCL to be dissolved.

Accordingly, the origin of the improved solvent resistance of the electrospun mat must rely on different size and distribution of the non-cross-linked areas of the sample. The size of the spherulites in the 3D printing, film, and MEW samples was large (as they were superstructural aggregates with radial lamellae inside them), in comparison with the solution electrospinning sample, where no spherulites were formed, and the morphology was characterized by oriented Shish-Kebabs formed by thin lamellae. This morphology was highly anisotropic, and many chains were oriented along the nanofiber axis inter dispersed with amorphous regions where the epoxy resin formed covalent links with the PCL chains. Due to refined oriented morphology (Shish-Kebab structures) in the samples obtained by solution electrospinning, the epoxy/PCL interface, where the exchange reaction mainly took place, was larger, and therefore the fibers were able to maintain their integrity when the soluble part was removed.

It is clear that the crystalline morphology of the electrospun fibers significantly improved the solvent resistance of the material. In order to check the solvent stability at temperatures higher than the melting of the fibers, the SEM images of the sample after the gel content determination experiment (1 h in chloroform at 100 °C and 200 Psi in the microwave extractor) were analysed (Fig. 7).

As shown in Fig. 7, the morphology of the nanofibers was maintained

**Table 2**
Melting temperature (Tm) and crystallinity degree (Xc) for the first and second heating scan for uncured and cured samples and pure PCL.

| | Before curing | | | | After curing | | | |
|---|---|---|---|---|---|---|---|---|
| | First scan | | Second scan | | First scan | | Second scan | |
| Sample | Tm (°C) | Xc (%)[a] | Tm (°C) | Xc (%)[a] | Tm (°C) | Xc (%)[a] | Tm (°C) | Xc (%)[a] |
| Solution electrospinning | 50 | 51 | 45 | 44 | 63 | 60 | 52 | 32 |
| MEW | 47 | 55 | 41 | 37 | 62 | 65 | 48 | 31 |
| Bulk film | 45 | 55 | 41 | 44 | 63 | 66 | 53 | 36 |
| 3D printing | 44 | 47 | 42 | 31 | 54 | 46 | 54 | 30 |
| Neat PCL | 63 | 65 | 55 | 44 | | | | |

[a] All the values are normalized by the PCL amount.

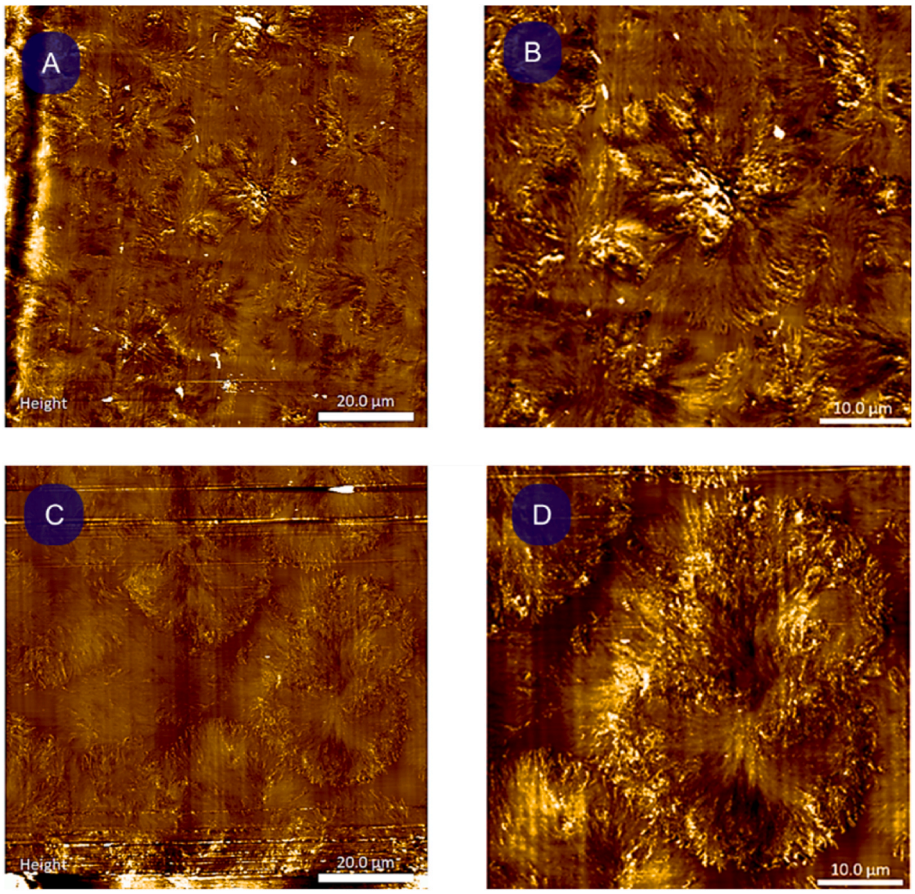


**Fig. 4.** AFM image of cured samples processed by MEW technique Height (A, B) and 3D printing technique Height (C, D).

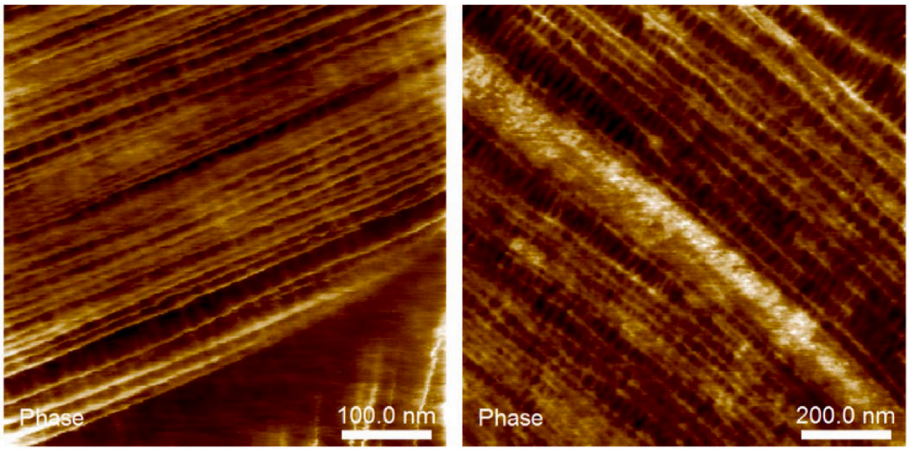


**Fig. 5.** AFM image of the cured electrospun sample.

after the solvent treatment at high temperature. This result shows that the fiber morphology remained even at temperatures higher than the melting of the PCL segments of the blend. To explain this behaviour, it should be considered that the epoxy curing confined the crystalline regions of the PCL, and because of that, the fiber-like morphology was maintained in the molten state.

According to the solvent swelling experiments, the electrospun mats could have application as solvent sensors. With the aim of exploring this application, solvent sorption experiments were carried out. The solubility of three solvent vapours, chloroform ($Pv_0$ = 194 mm Hg), acetone ($Pv_0$ = 230 mm Hg), and water ($Pv_0$ = 24 mm Hg) to activity 1 at 25 °C was studied (Fig. 8). They are represented in terms of the percentage of solvent vapor absorbed at equilibrium versus solvent vapor activity (a = $P/Pv_0$).

As observed, the behaviour was dramatically different for each solvent, especially at activity values higher than 0.3. Although the cured mats did not show a clear Tg in DSC, it could be considered that they were in the glassy state at 25 °C. Therefore, the phenomenology of the process could be described by the dual model, which assumes that part of the penetrant adsorbs on the walls of the material adjacent to the free volume, while another population of the penetrant dissolves in the polymer matrix [29]. However, this behaviour was not observed in the

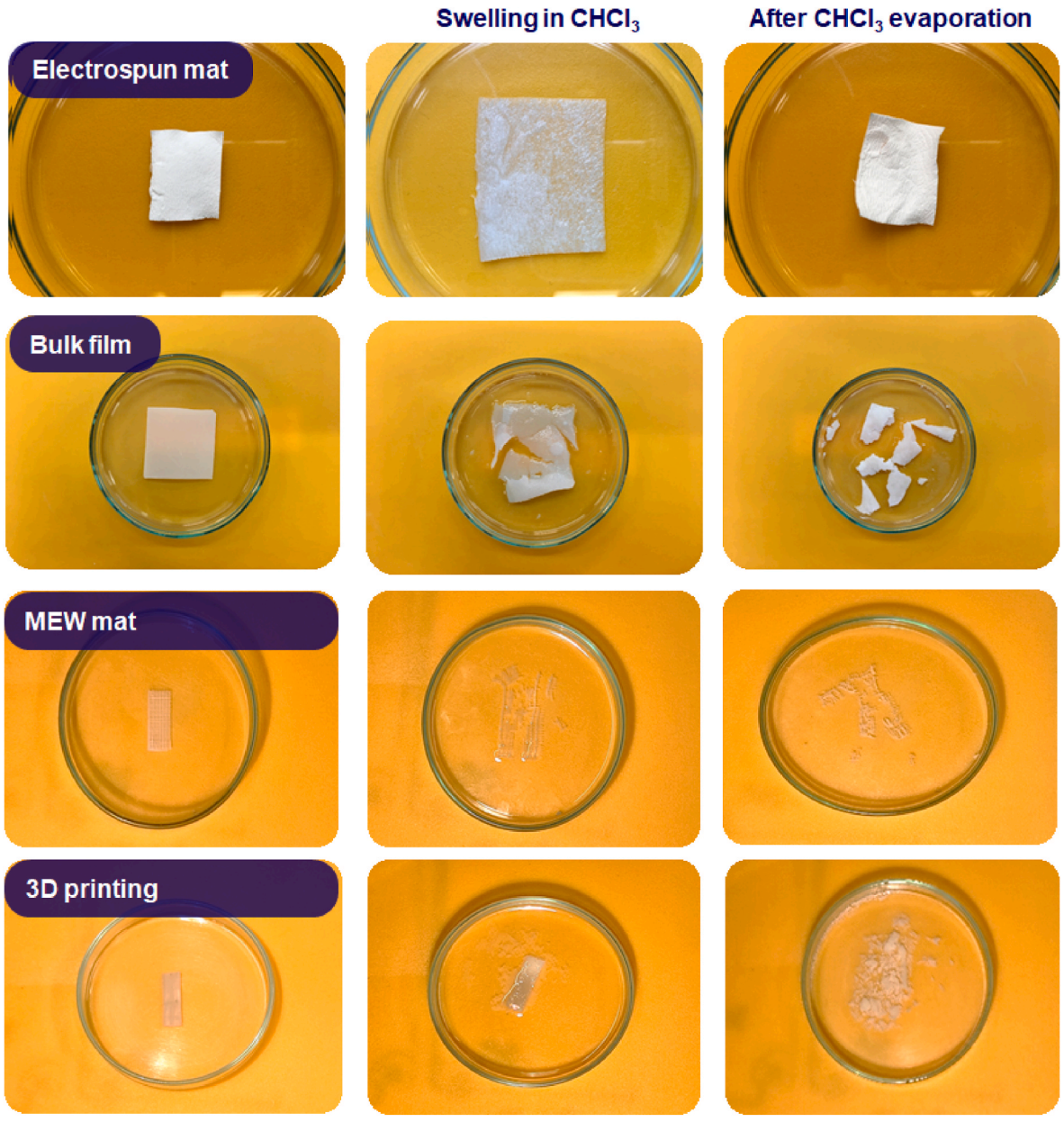


**Fig. 6.** Images of the cured samples processed by the different techniques before, after swelling in chloroform and after solvent evaporation. (Video 1 shows the swelling process for the electrospun mat).

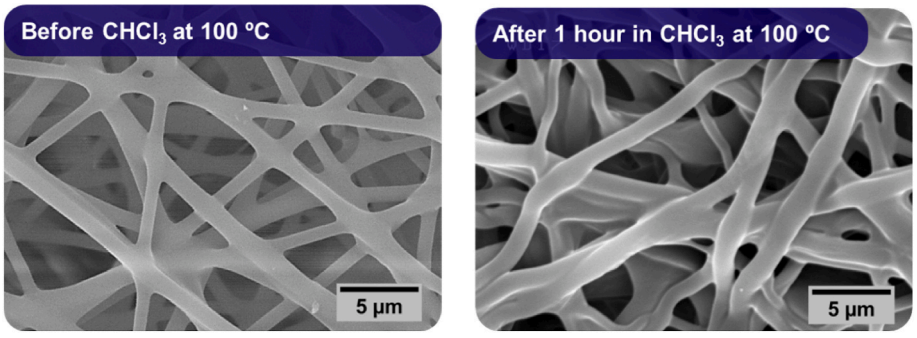


**Fig. 7.** SEM image of electrospun mat before and after 1 h in $CHCl_3$ at 100 °C and 200 Psi.

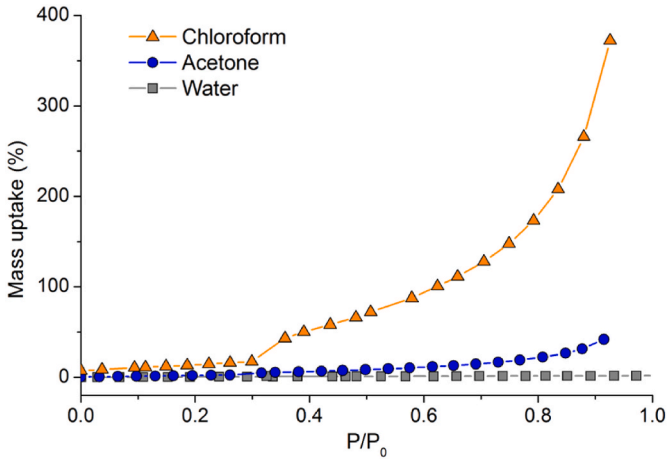


**Fig. 8.** Sorption isotherms at 25 °C for cured electrospun mats.

experiments. Thus, when the mat was exposed to water vapor, a linear dependence was observed in the activity range that was studied, so the solubility of water in the polymer did not depend on the vapor pressure. This fact showed that there was little interaction between the polymer and the water due to the high hydrophobicity of the polymer. In the case of the sample exposed to acetone vapor, a similar behaviour was observed up to 0.7 activity, after which the amount of penetrant absorbed into the polymer increased as a function of the vapor pressure.

Finally, it was observed that the amount of chloroform absorbed at equilibrium showed a linear dependence up to 0.3 activity, and after this value, a very large increase of the activity with vapor pressure was registered. This result was a consequence of the high affinity between the chloroform and the polymer. In the case of vapours with high interactions with the polymer, the sorption mechanism is different from the dual model and involves the classical swelling of the polymer by the penetrant. In this case, the chloroform sorption was well explained by the Flory-Huggings theory [30]. This theory also justified the behaviour observed in acetone, although to a lesser extent.

To summarize, the electrospun mats presented very high affinity towards chloroform as they absorbed up to four hundred times their weight. In addition, in chloroform the integrity of the mesh was maintained as shown in Fig. 6. Therefore, the electrospun mats present potential applications as chloroform sensors.

### 3.5. Shape memory

Shape memory qualitative experiments were performed for the samples obtained by solution electrospinning [18], solution casting, and melt electrowriting were performed and the results are shown in videos 2,3,4 and Fig. S3. As observed these samples presented shape memory properties. Shape memory properties were also analysed by DMA in tensile mode for three consecutive cycles. The results for the electrospun mat are shown in Fig. 9 and for the others samples are shown in Fig. S4.

Fig. 9 shows that the sample was able to fix a temporal shape at 70 °C after heating and cooling and recover the initial shape when heated again at 70 °C. This result evidenced that the PCL melting allowed the sample to adopt a temporal shape that was fixed after the crystallization when the sample was cooled. However, when the sample was heated, it recovered the shape because of the elastic restoration of the crosslinked structure. The same experiment was performed for the samples obtained by the different processing techniques. Table 3 shows the fixity and recovery ratio for the samples processed with different techniques.

As shown in Table 3, the sample obtained by 3D printing did not present shape memory properties. As this sample was thicker than the others, it was assumed that the higher sample thickness reduced the shape memory abilities. However, thinner samples were printed (0.5 mm) but no shape memory properties were obtained. Different printing geometries were also tested such as printing the sample in the DMA test direction, but no improvements were obtained. Therefore, it could be argued that the 3D printed sample was not able to fix a shape because of the poor interlayer adhesion. Therefore, when the sample was exposed

**Table 3**
Fixity and recovery ratios for the samples processed by different techniques.

| Manufacturing technique | Fixity (%) (1°/2°/3° cycle) | Recovery (%) (1°/2°/3° cycle) |
|---|---|---|
| Electrospinning | 96/95/97 | 95/99/99 |
| MEW | 93/92/91 | 71/88/98 |
| Bulk film | 95/90/90 | 74/99/99 |
| 3D printing | – | – |

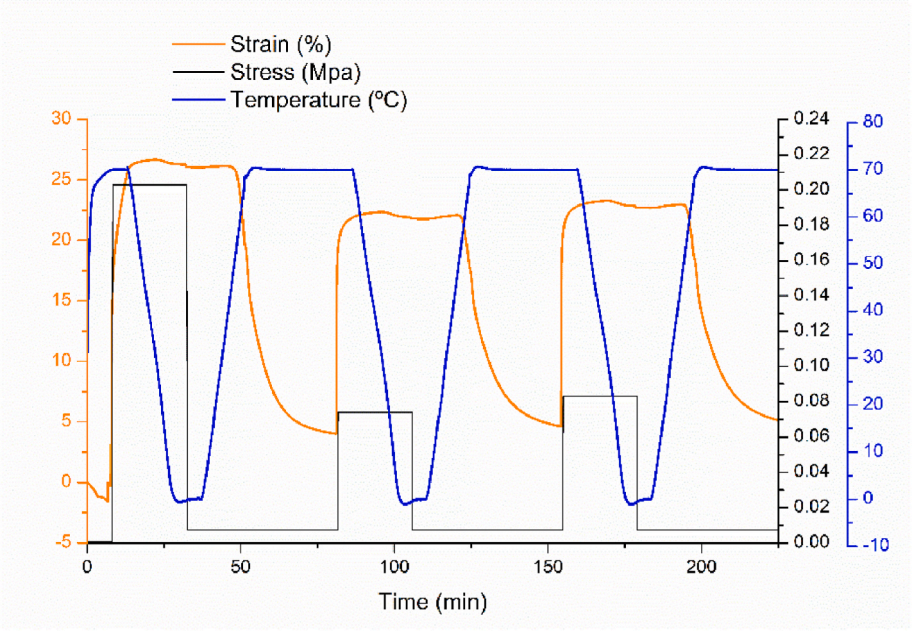


**Fig. 9.** Dynamical mechanical thermal analysis (DMA) shape memory test for electrospun mats.

to UV irradiation, the crosslinking process happened in each layer, reducing the interlayer adhesion. This layer-by-layer crosslinking that occurred because of the poor adhesion caused the thermosetting network formed for the 3D sample to be different compared to other samples, and the sample did not present shape memory properties.

However, as shown in Table 3, the mats obtained by solution electrospinning, MEW, and bulk films presented shape memory properties. This fact was related to the phase-separated structure of the blend described by DSC. The highly phase-separated PCL segments play a key role in the shape memory property of the blend as their melting/crystallization abilities are the switching elements that enable the temporal shape to be fixed. It is worth mentioning that regardless of the cycle, the sample obtained by solution electrospinning presented the highest fixity ratio. This result was related to the morphology of the material. As the solution electrospun mat was composed of many nanofibers, it could be more adaptable to new temporal shapes.

In addition, the solution electrospun mat showed a better recovery ratio. According to the literature [31], residual strain in the electrospun sample which is recovered in the first shape memory cycle, could counterbalances any plastic deformation. To study this effect, the electrospun mat was thermally annealed for 10 min at 70 °C but no shrinkage was observed (Fig. S5). Accordingly, this effect was discarded, and it was stated that the electrospun mat presented less permanent plastic deformation. This result could not be explained considering a higher crosslinking degree since the conversion of the epoxy crosslinking reaction and gel content of all the samples was similar. It was considered that the Shish-Kebab type morphology induced during the strong elongational flow produced by the electrospinning process could be responsible for this behaviour. As shown in the AFM images, in this sample, PCL chains formed flow-oriented crystals (Shish) that acted as nucleation points for other lamellar crystals (Kebab), while in the other samples, PCL chains crystallized within isotropic spherulites (composed of radially oriented lamellae). The epoxy resin formed a phase-separated structure, and it was probably in close contact with the amorphous phase of the PCL. As the transesterification reaction between the epoxy and the PCL only happened in the amorphous phase of the PCL, it can be argued that the distribution of the joining points between the epoxy and the PCL chains was different when the sample presented a Shish-Kebab or spherulitic morphology. Accordingly, in the shish-kebab type morphology, the morphology was highly anisotropic, and many chains were oriented along the nanofiber axis inter dispersed with amorphous regions where the epoxy resin formed covalent links with the PCL chains. As the PCL crystals melted, the elastic recovery of the epoxy network was higher, as most of the chains were also oriented along the nanofiber axis.

Finally, considering the high affinity of the electrospun mat towards solvent and the dimensional stability of the samples, chloroform was used to trigger the shape memory recovery. The result of this experiment is shown in video 5, and as observed, the electrospun mat was able to recover the original shape after chloroform immersion.

## 4. Conclusions

DGEBA/PCL blends could be processed by different manufacturing techniques such as casting, solution electrospinning, MEW, and 3D printing. The blends were crosslinked by cationic photopolymerization, and high curing degree networks were obtained. As observed by DSC, the cured blend was phase separated. Gel content measurements showed that the PCL was integrated into the epoxy network because of the occurrence of transesterification reactions.

The high elongation forces present in the solution electrospinning process produced Shish-Kebab-type crystalline morphology in the electrospun fibers, while all the other samples presented a spherulitic morphology. The Shish-Kebab morphology was highly anisotropic, and many chains were oriented along the nanofiber axis inter dispersed with amorphous regions where the epoxy resin formed covalent links with the PCL chains. Thanks to this morphology, the electrospun mats presented excellent solvent resistance and could have potential applications as chloroform sensors.

All the samples except the 3D-printed one presented shape memory abilities. The poor interlayer adhesion of the 3D printed sample prevented the fixation of a temporal shape. Solution electrospun mats presented the best fixity and recovery ratios. This was attributed, on the one hand, to the fiber type morphology, which made the sample more adaptable to new temporal shapes, and on the other hand, to a higher elastic recovery induced by the orientation of the polymer chains in the fiber direction, characteristic of the Shish-Kebab morphology.

## CRediT authorship contribution statement

**I. Razquin:** Investigation, Visualization, Writing – original draft. **A. Iregui:** Investigation, Writing – original draft. **M. Cobos:** Investigation. **J. Latasa:** Investigation, Writing – review & editing. **A. Eceiza:** Writing – review & editing. **K. González:** Investigation. **L. Martin:** Investigation, Writing – review & editing. **A.J. Müller:** Funding acquisition, Writing – review & editing. **A. González:** Conceptualization, Funding acquisition, Investigation, Project administration, Supervision, Visualization, Writing – original draft, Writing – review & editing. **L. Irusta:** Conceptualization, Funding acquisition, Investigation, Project administration, Supervision, Writing – original draft, Visualization, Writing – review & editing.

## Declaration of competing interest

The authors declare that they have no known competing financial interests or personal relationships that could have appeared to influence the work reported in this paper.

## Data availability

Data will be made available on request.

## Acknowledgements

AJM acknowledges funding by the Basque Government through grant IT1503-22. LI acknowledges funding by the Basque Government through grant IT1667-22.

## Appendix A. Supplementary data

Supplementary data to this article can be found online at https://doi.org/10.1016/j.polymer.2023.126160.

## References

[1] B. Lester, T. Baxevanis, Y. Chemisky, D. Lagoudas, B. Lester, T. Baxevanis, Y. Chemisky, L. Dimitris, Review and perspectives : shape memory alloy composite systems to cite this version : science arts & métiers (SAM), Acta Mech. 226 (2015) 3907–3960.

[2] M.D. Hager, S. Bode, C. Weber, U.S. Schubert, Shape memory polymers: past, present and future developments, Prog. Polym. Sci. 49–50 (2015) 3–33, https://doi.org/10.1016/j.progpolymsci.2015.04.002.

[3] Y. Lu, H. Xu, N. Liang, Z. Xu, S. Chen, D. Zhang, High mechanical strength of shape-memory hyperbranched epoxy resins, ACS Appl. Polym. Mater. 4 (2022) 5574–5582, https://doi.org/10.1021/acsapm.2c00625.

[4] B.Q.Y. Chan, Z.W.K. Low, S.J.W. Heng, S.Y. Chan, C. Owh, X.J. Loh, Recent advances in shape memory soft materials for biomedical applications, ACS Appl. Mater. Interfaces 8 (2016) 10070–10087, https://doi.org/10.1021/acsami.6b01295.

[5] F. Pilate, A. Toncheva, P. Dubois, J.M. Raquez, Shape-memory polymers for multiple applications in the materials world, Eur. Polym. J. 80 (2016) 268–294, https://doi.org/10.1016/j.eurpolymj.2016.05.004.

[6] I. Razquin, A. Iregui, L. Orduna, L. Martin, A. González, L. Irusta, Reprogrammable permanent shape memory materials based on reversibly crosslinked epoxy/PCL blends, Molecules 25 (2020) 1–16, https://doi.org/10.3390/molecules25071568.

[7] J. Karger-Kocsis, S. Kéki, Review of progress in shape memory epoxies and their composites, Polymers 10 (2017) 1–38, https://doi.org/10.3390/polym10010034.

[8] S. Zheng, H. Zheng, Q. Guo, Epoxy resin/poly(ε-caprolactone) blends cured with 2,2-bis[4-(4-aminophenoxy)phenyl]propane. I. Miscibility and crystallization kinetics, J. Polym. Sci., Part B: Polym. Phys. 41 (2003) 1085–1098, https://doi.org/10.1002/polb.10435.
[9] J. Zhang, T. Lin, S.C.P. Cheung, C.H. Wang, The effect of carbon nanofibres on self-healing epoxy/poly(ε-caprolactone) blends, Compos. Sci. Technol. 72 (2012) 1952–1959, https://doi.org/10.1016/j.compscitech.2012.08.017.
[10] Q. Guo, G. Groeninckx, Crystallization kinetics of poly(ε-caprolactone) in miscible thermosetting polymer blends of epoxy resin and poly(ε-caprolactone), Polymer (Guildf) 42 (2001) 8647–8655, https://doi.org/10.1016/S0032-3861(01)00348-2.
[11] D. Yuan, V.S. Bonab, A. Patel, I. Manas-Zloczower, Self-healing epoxy coatings with enhanced properties and facile processability, Polymer (Guildf) 147 (2018) 196–201, https://doi.org/10.1016/J.POLYMER.2018.06.017.
[12] A. Iregui, L. Irusta, L. Martin, A. González, Analysis of the process parameters for obtaining a stable electrospun process in different composition epoxy/poly ε-Caprolactone blends with shape memory properties, Polymers 11 (2019) 475, https://doi.org/10.3390/polym11030475.
[13] A. Dorigato, D. Rigotti, A. Pegoretti, Novel poly(caprolactone)/epoxy blends by additive manufacturing, Materials 13 (2020), https://doi.org/10.3390/ma13040819.
[14] J.L. Chen, F.C. Chang, Phase separation process in poly(e-caprolactone)-epoxy blends, Macromolecules 32 (1999) 5348–5356, https://doi.org/10.1021/ma981819o.
[15] H. Lützen, T.M. Gesing, B.K. Kim, A. Hartwig, Novel cationically polymerized epoxy/poly(ε-caprolactone) polymers showing a shape memory effect, Polymer (Guildf) 53 (2012) 6089–6095, https://doi.org/10.1016/j.polymer.2012.10.033.
[16] T. Tsujimoto, T. Takayama, H. Uyama, Biodegradable shape memory polymeric material from epoxidized soybean oil and polycaprolactone, Polymers 7 (2015) 2165–2174, https://doi.org/10.3390/polym7101506.
[17] Á. Iregui, I. Otaegi, I. Arandia, M.D. Martin, A.J. Müller, L. Irusta, A. González, Fully reversible spherulitic morphology in cationically photopolymerized DGEBA/PCL shape-memory blends, Macromolecules 53 (2020) 1368–1379, https://doi.org/10.1021/acs.macromol.9b02474.
[18] A. Iregui, L. Irusta, O. Llorente, L. Martin, T. Calvo-Correas, A. Eceiza, A. González, Electrospinning of cationically polymerized epoxy/polycaprolactone blends to obtain shape memory fibers (SMF), Eur. Polym. J. 94 (2017) 376–383, https://doi.org/10.1016/j.eurpolymj.2017.07.026.
[19] Y.M. Kim, L. Kris Kostanski, J.F. MacGregor, Kinetic studies of cationic photopolymerizations of cycloaliphatic epoxide, triethyleneglycol methyl vinyl ether, and cyclohexene oxide, Polym. Eng. Sci. 45 (2005) 1546–1555, https://doi.org/10.1002/pen.20383.
[20] J. Parameswaranpillai, S.K. Sidhardhan, S. Jose, N. Hameed, N.V. Salim, S. Siengchin, J. Pionteck, A. Magueresse, Y. Grohens, Miscibility, phase morphology, thermomechanical, viscoelastic and surface properties of poly (ε-caprolactone) modified epoxy systems: effect of curing agents, Ind. Eng. Chem. Res. 55 (2016) 10055–10064, https://doi.org/10.1021/acs.iecr.6b01713.
[21] A. Arnebold, S. Wellmann, A. Hartwig, Network dynamics in cationically polymerized, crosslinked epoxy resins and its influence on crystallinity and toughness, Polymer (Guildf) 91 (2016) 14–23, https://doi.org/10.1016/j.polymer.2016.03.052.
[22] J.M. Morancho, A. Cadenato, X. Ramis, M. Morell, X. Fernández-Francos, J. M. Salla, A. Serra, Unexpected differences between thermal and photoinitiated cationic curing of a diglycidyl ether of bisphenol A modified with a multiarm star poly(styrene)-b-poly(ε-caprolactone) polymer, Express Polym. Lett. 7 (2013) 565–576, https://doi.org/10.3144/expresspolymlett.2013.54.
[23] Q. Guo, C. Harrats, G. Groeninckx, H. Reynaers, M.H.J. Koch, Miscibility, crystallization and real-time small-angle X-ray scattering investigation of the semicrystalline morphology in thermosetting polymer blends, Polymer (Guildf) 42 (2001) 6031–6041, https://doi.org/10.1016/S0032-3861(01)00093-3.
[24] X. Luo, R. Ou, D.E. Eberly, A. Singhal, W. Viratyaporn, P.T. Mather, A Thermoplastic/Thermoset Blend Exhibiting Thermal Mending and Reversible Adhesion, 2009, https://doi.org/10.1021/am8001605.
[25] R.H. Somani, L. Yang, L. Zhu, B.S. Hsiao, Flow-induced shish-kebab precursor structures in entangled polymer melts, Polymer (Guildf) 46 (2005) 8587–8623, https://doi.org/10.1016/j.polymer.2005.06.034.
[26] A.W. Monks, H.M. White, D.C. Bassett, On shish-kebab morphologies in crystalline polymers, Polymer (Guildf) 37 (1996) 5933–5936, https://doi.org/10.1016/S0032-3861(96)00626-X.
[27] M. Trujillo, M.L. Arnal, A.J. Müller, M.A. Mujica, C. Urbina De Navarro, B. Ruelle, P. Dubois, Supernucleation and crystallization regime change provoked by MWNT addition to poly(ε-caprolactone), Polymer (Guildf) 53 (2012) 832–841, https://doi.org/10.1016/j.polymer.2011.12.028.
[28] C.T. Lim, E.P.S. Tan, S.Y. Ng, Effects of crystalline morphology on the tensile properties of electrospun polymer nanofibers, Appl. Phys. Lett. 92 (2008), 141908, https://doi.org/10.1063/1.2857478.
[29] R.M. Barrer, Diffusivities in glassy polymers for the dual mode sorption model, J. Membr. Sci. 18 (1984) 25–35, https://doi.org/10.1016/S0376-7388(00)85023-1.
[30] A. Etxeberria, C. Etxabarren, J.J. Iruin, Comparison between Static (Sorption) and Dynamic (IGC) Methods in the Determination of Interaction Parameters in Polymer/Polymer Blends, 2000, https://doi.org/10.1021/ma992173i.
[31] B. Peng, Y. Yang, T. Ju, K.A. Cavicchi, Fused filament fabrication 4D printing of a highly extensible, self-healing, shape memory elastomer based on thermoplastic polymer blends, ACS Appl. Mater. Interfaces 13 (2021) 12777–12788, https://doi.org/10.1021/acsami.0c18618.